ANO2 is the cilial calcium-activated chloride channel that may mediate olfactory amplification

Aaron B. Stephan[a], Eleen Y. Shum[a], Sarah Hirsh[a], Katherine D. Cygnar[a], Johannes Reisert[b,1], and Haiqing Zhao[a,1]

[a]Department of Biology, The Johns Hopkins University School of Medicine, 3400 N Charles Street, Baltimore, MD 21218; and [b]Monell Chemical Senses Center, 3500 Market Street Philadelphia, PA 19104-3308

Edited by Jeremy Nathans, Johns Hopkins University School of Medicine, Baltimore, MD, and approved May 18, 2009 (received for review March 31, 2009)

For vertebrate olfactory signal transduction, a calcium-activated chloride conductance serves as a major amplification step. However, the molecular identity of the olfactory calcium-activated chloride channel (CaCC) is unknown. Here we report a proteomic screen for cilial membrane proteins of mouse olfactory sensory neurons (OSNs) that identified all the known olfactory transduction components as well as Anoctamin 2 (ANO2). *Ano2* transcripts were expressed specifically in OSNs in the olfactory epithelium, and ANO2::EGFP fusion protein localized to the OSN cilia when expressed in vivo using an adenoviral vector. Patch-clamp analysis revealed that ANO2, when expressed in HEK-293 cells, forms a CaCC and exhibits channel properties closely resembling the native olfactory CaCC. Considering these findings together, we propose that ANO2 constitutes the olfactory calcium-activated chloride channel.

Anoctamin | cilia | olfaction | signal transduction | TMEM16B

In the nervous system, chloride conductances often serve critical signaling roles, functioning as either inhibitory or excitatory signals. In vertebrate olfactory sensory neurons (OSNs), signaling by a calcium-activated chloride conductance in the cilia is the final step of a well-characterized signal transduction pathway (1, 2). Because of the active accumulation of chloride within OSNs (3–5), this chloride conductance (6–9) serves as an amplification step, accounting for up to 80% to 90% of the odorant-induced depolarizing current (10–12) and thus is critical for olfactory sensation. In this study, we identified Anoctamin 2 (ANO2) in a proteomic screen of OSN cilial membranes. We provide molecular and electrophysiological evidence indicating that ANO2 constitutes the long-sought olfactory calcium-activated chloride channel (CaCC) that may mediate signal amplification.

Results

ANO2 Is Present in a Preparation of Olfactory Cilial Membranes. In rodents, the native olfactory CaCC is predicted to be 8 times more abundant than the olfactory cationic cyclic nucleotide-gated (CNG) channel (9). Because of this high abundance, we reasoned that a proteomic screen might be a viable approach to identify this channel. Therefore, we isolated OSN cilia from mouse olfactory mucosa, enriched the preparation for membrane proteins, and separated the proteins by SDS/PAGE (Fig. S1). To reduce the potential interference in the proteomic analysis by odorant receptors (ORs), which include more than 1000 different types and usually migrate at 35–55 kDa, we cut the gel into 3 slices: $>$ 55 kDa, 35–55 kDa, and $<$35 kDa, and analyzed each slice by mass spectrometry. We performed 2 independent cilial membrane preparations and mass spectrometric screens. Only proteins that were identified by 2 or more peptides in both preparations were considered for further analysis.

Because most chloride channels have several transmembrane domains and therefore are of a larger molecular weight (Fig. S2), we initially focused our analysis on the $>$ 55-kDa sample, in which 53 proteins were identified (Table 1 and Table S1). The robustness of this approach was confirmed by the identification of all known transmembrane and membrane-associated olfactory transduction components downstream of ORs within this range of molecular weights (Table 1). Other proteins arising from OSNs, e.g., the neural cell adhesion molecule 1, were found also. In addition, a number of proteins from dominant contaminating sources, i.e., axonemes (tubulin) and microvilli of sustentacular cells (cytochrome P450 2A; ref. 13) were present.

Because we had found all of the known signal transduction components downstream of ORs, we reasoned that the olfactory CaCC likely should be included in this short list of 53 proteins. We thus narrowed the candidates for the olfactory CaCC down to 2 categories of proteins: those annotated to confer a chloride conductance and those predicted to be transmembrane proteins with unknown function. Only 3 proteins, CLIC6, TMEM16B (ANO2), and Q8BH53, were found in these 2 categories. CLIC6 is a member of a family of intracellular chloride channels (14). However, in situ hybridization showed that CLIC6 is expressed primarily in supporting cells in the olfactory epithelium (OE), but not in OSNs (Fig. S3). Q8BH53 (gi81896083) is a protein of unknown function. It is enriched in many ciliated cells (15), and might have a more general role in cilial structure or maintenance.

TMEM16B (ANO2) is 1 of 10 members of the Anoctamin family of proteins (16). ANO2 is predicted to have 8 transmembrane domains with both N and C termini in the cytoplasm, a topology consistent with many ion channels. A mutation in human TMEM16E (ANO5) causes gnathodiaphyseal dysplasia, a disorder characterized by bone calcification defects (17). Bone calcification defects have been noted for mutations in chloride channels (18). BLAST (http://www.ncbi.nlm.nih.gov/BLAST/) searches revealed that ANO family members are related to the yeast protein Ist2p. Mutants of Ist2p were reported to have increased tolerance to NaCl (19). These studies, as well as our identification of ANO2 in the olfactory cilial proteomic screen, pointed to ANO2 as a promising candidate for the olfactory CaCC.

Olfactory Sensory Neurons Express a Splice Variant of *Ano2*. *Ano2* transcripts are highly expressed in the olfactory system (GNF Symatlas and Genepaint), specifically in OSNs (20). Using independent in situ hybridization probes, we confirmed that *Ano2* mRNA localized specifically to OSNs within the OE and not to the sustentacular or basal stem cell layers (Fig. 1*A*).

To date, mouse *Ano2* mRNA sequences available from online databases are derived from retinal cDNA. The Ensembl database predicts several *Ano2* transcript variants with different transcription initiation sites. We characterized mouse olfactory *Ano2* transcripts. The longest ORF obtained by RT-PCR was 2,730 bases, made of 24 exons (see *SI Methods* for details). We

Author contributions: A.B.S., J.R., and H.Z. designed research; A.B.S., E.Y.S., S.H., K.D.C., J.R., and H.Z. performed research; A.B.S. and J.R. analyzed data; and A.B.S., J.R., and H.Z. wrote the paper.

The authors declare no conflict of interest.

This article is a PNAS Direct Submission.

Freely available online through the PNAS open access option.

[1]To whom correspondence may be addressed. E-mail: hzhao@jhu.edu or jreisert@monell.org.

This article contains supporting information online at www.pnas.org/cgi/content/full/0903304106/DCSupplemental.

Table 1. Proteins identified by mass spectrometry

Symbol	Protein Name	GI Accession Number	Peptides Average (first, second)
ATP1A1	sodium/potassium ATPase alpha-1	55976751	35 (30, 40)
P450R	NADPH cytochrome P450 reductase	548338	30 (25, 35)
ANXA6	annexin a6	113963	20.5 (19, 22)
AC3	**adenylyl cyclase type 3**	**25008337**	**18 (14, 22)**
VIL2	Ezrin	32363497	14.5 (20, 9)
HSPA5	glucose-regulated protein 78	2506545	14 (9, 19)
HSC70C	Heat-shock cognate 71-kDa protein 8	51702275	13 (10, 16)
NCAM1	neural cell adhesion molecule 1	205830666	12.5 (6, 19)
ATP6V1A	vacuolar ATP synthase catalytic subunit a	145559539	12.5 (16, 9)
ANPEP	aminopeptidase n	31077182	12.5 (17, 8)
TBB3	tubulin beta-3	20455323	11.5 (12, 11)
SLC27A2	very-long-chain acyl-CoA synthetase	3183203	11 (11, 11)
ENPL	Heat-shock protein 90-kDa beta 1	119362	11 (10, 12)
TMEM16B	*transmembrane protein 16B (Anoctamin-2)*	*81877094*	*10.5 (12, 9)*
VOME	vomeromodulin	81895337	10.5 (5, 16)
PDE1C	**phosphodiesterase 1c**	**57015315**	**10 (12, 8)**
TBA1A	tubulin alpha-1	55977479	10 (11, 9)
Q8BH53	*hypothetical transmembrane protein*	*81896083*	*9.5 (10, 9)*
MYO6	myosin-6	13431710	9 (4, 14)
ECHA	trifunctional enzyme subunit alpha, mitochondrial	81874329	8 (5, 11)
STOM	stomatin	122066246	7 (3, 11)
TERA	transitional endoplasmic reticulum ATPase	146291078	7 (10, 4)
CNGA2	**cyclic nucleotide-gated channel A2**	**2493744**	**6.5 (5, 8)**
CP2A5	cytochrome P450 2a5	117196	5.5 (6, 5)
CP2A4	cytochrome P450 2a4	117195	5.5 (5, 8)
4F2HC	4f2 cell-surface antigen heavy chain	112804	5.5 (4, 7)
NKCC1	**sodium- (potassium)-chloride cotransporter 1**	**1709293**	**5.5 (4, 7)**
CMC1	mitochondrial aspartate glutamate carrier 1	47605479	5 (3, 7)
AL3B1	aldehyde dehydrogenase 3b1	67460523	5 (7, 3)
CTNA1	alpha-1 catenin	117607	5 (4, 6)
AT1A2	sodium/potassium ATPase alpha-2	66773992	4.5 (6, 3)
CLIC6	*chloride intracellular channel 6*	*46395841*	*4.5 (6, 3)*
ALBU	serum albumin precursor	5915682	4 (4, 4)
UD2A2	UDP glucuronosyltransferase 2a2	81892490	4 (6, 2)
HS90A	Heat-shock protein 90-alpha	1170384	4 (3, 5)
LRGUK	guanylate kinase domain-containing protein	81905373	3.5 (4, 3)
DCDC2	doublecortin domain-containing protein 2	71153322	3.5 (2, 5)
CNGB1.B	**cyclic nucleotide-gated channel B1.b**	**81895348**	**3.5 (4, 3)**
TBB4	tubulin beta-4	146345529	3.5 (5, 2)
AT1B1	sodium/potassium-ATPase beta-1	114393	3 (2, 4)
ODP2	dihydrolipoamide acetyltransferase homolog	146325018	3 (3, 3)
AQP1	aquaporin-1	543832	3 (3, 3)
AT12A	proton/potassium ATPase alpha chain 2	51338843	3 (2, 4)
CD36	platelet glycoprotein 4	729081	3 (4, 2)
CLH	clathrin heavy chain	66773801	3 (3, 3)
TKT	transketolase	730956	3 (4, 2)
ANXA1	annexin a1	113945	2.5 (3, 2)
HS71A	Heat-shock 70-kDa protein 1a	56757667	2.5 (2, 3)
Q9WV19	olfactory-specific cytochrome P450 2 g1	81907639	2 (2, 2)
ABCB6	ATP-binding cassette, sub-family b, member 6	81917203	2 (2, 2)
NCKX4	sodium/potassium/calcium exchanger 4	37081103	2 (2, 2)
Q9ESE4	olfactor UDP glucuronosyltransferase	81906316	2 (2, 2)
SO1A1	sodium-independent organic anion- transporter 1	27734565	2 (2, 2)

List of 53 proteins from the > 55-kDa sample. Listings in bold are proteins known to be involved in olfactory transduction (1, 2). Listings in italics are proteins either annotated to confer chloride conductance or with no known function. For the full list of identified proteins of all molecular weights, including the lower molecular weight olfactory transduction components ($G\alpha_{olf}$ and CNGA4), see Table S1.

found that the retinal exon 13, which encodes 4 amino acids in the predicted first intracellular loop, is absent in the olfactory-specific isoform (Fig. 1 *B* and *C*), suggesting that OSNs express a splice variant. The functional significance of these 4 missing amino acids remains to be determined. We also found that ANO2 exon 3, which encodes 33 amino acids in the predicted N-terminal cytoplasmic domain, is lacking in a minority of transcripts in both OSNs and retinal cells (Fig. 1*D*). Translation of the major isoform of the olfactory-specific *Ano2* ORF yields 909 amino acids, with a predicted molecular weight of 104 kDa.

ANO2::EGFP Fusion Protein Traffics to Olfactory Cilia. If ANO2 functions as the olfactory CaCC, it should be located in the OSN cilia. To determine whether the ANO2 protein found in the

NEUROSCIENCE

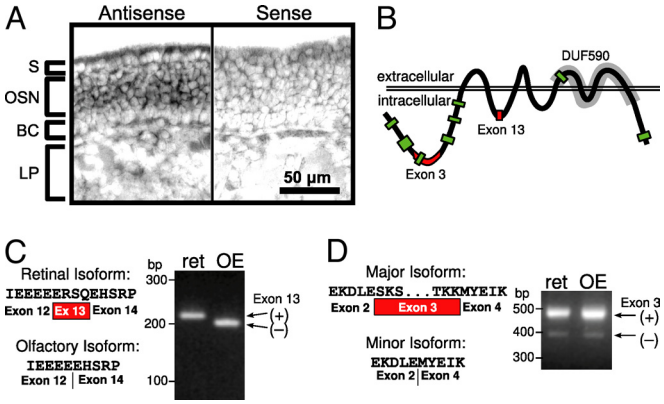

Fig. 1. Analysis of ANO2 transcripts. (*A*) In situ hybridization for *Ano2* in mouse OE. BC, basal cells; LP, lamina propria; OSN, olfactory sensory neurons; S, sustentacular cells. (*B*) Schematic of ANO2 predicted transmembrane topology. Green boxes indicate segments identified by mass spectrometry. Red boxes indicate segments encoded by exon 3 and the retinal exon 13. Gray highlights a conserved domain (DUF590) in all Anoctamin family members. (*C*) Exon 13 is present in the retinal isoform of *Ano2* but is absent in the olfactory isoform. (*Right*) RT-PCR analysis with primers spanning the Exon 13 site. ret, retinal cDNA; OE, olfactory epithelial cDNA. (*D*) The major *Ano2* isoforms in both retinal cells and OSNs contain exon 3, which is spliced out in a minor isoform. (*Right*) RT-PCR analysis with primers spanning the exon 3 site.

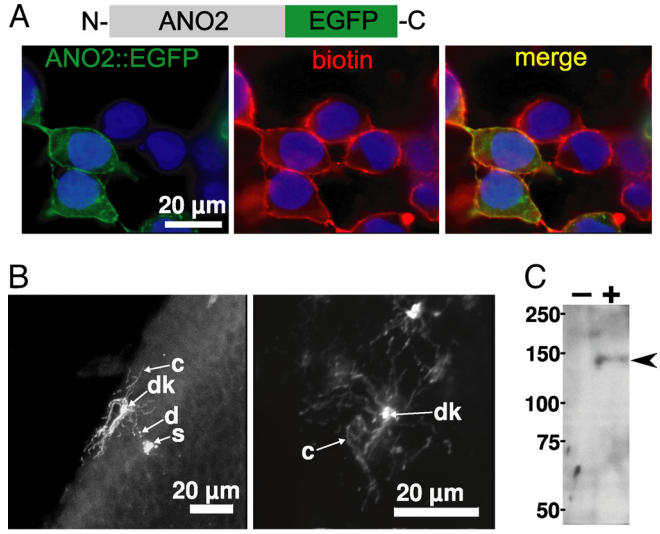

Fig. 2. Subcellular localization of ANO2::EGFP fusion proteins. (*A*) Anti-GFP immunostaining of HEK-293 cells transfected with the ANO2::EGFP plasmid. (*Left*) GFP staining shown in green. (*Center*) Cell surface labeling by biotinylation shown in red. (*Right*) The merge. Cell nuclei were counterstained with DAPI shown in blue. (*B*) Immunostaining of OE infected with an adenovirus expressing ANO2::EGFP using an anti-GFP antibody. (*Left*) Side view of a virus-infected OSN. (*Right*) *En face* view of a virus-infected OSN. c, cilia; d, dendrite; dk, dendritic knob; s, soma. (*C*) Western blot analysis using an anti-GFP antibody on olfactory mucosal tissues either infected with the ANO2::EGFP adenovirus (+) or not infected (−). Arrowhead points to the sole ≈130-kDa band present in the infected tissue.

proteomic screen was indeed arising from OSN cilial membranes, we monitored the subcellular localization of GFP-tagged ANO2 proteins. We generated expression constructs for N- or C-terminally EGFP-tagged ANO2 (EGFP::ANO2 or ANO2::EGFP) and expressed them in HEK-293 cells. ANO2::EGFP localized to the plasma membrane (Fig. 2*A*). However, EGFP::ANO2 remained intracellular (Fig. S4). These data suggest that the signal sequence for trafficking of ANO2 to the plasma membrane may reside at the N terminus, in contrast to the yeast Ist2p that was reported to traffic to the plasma membrane by a C-terminal signal sequence (21).

We then generated an adenoviral vector to deliver DNA encoding ANO2::EGFP to OSNs in vivo. Low doses of virus were used to infect cells in the OE sparsely, allowing the clear visualization of individual OSNs. ANO2::EGFP localized primarily in the cilia and dendritic knobs of OSNs (Fig. 2*B*, Movie S1), a morphology reminiscent of those labeled by individual odorant receptor antibodies (22). Additionally, puncta of ANO2::EGFP were apparent in the dendrite, and there was perinuclear fluorescence in the OSN soma. No fluorescence was observed in the OSN axons. Western blot analysis confirmed that the ANO2::EGFP fusion protein of the expected size was present in the infected OE (Fig. 2*C*).

ANO2 Exhibits Channel Properties Similar to the Native Olfactory CaCC. Recently, ANO1 (TMEM16A), a paralog of ANO2, has been found to form a CaCC when heterologously expressed (23–25). ANO2 also was shown to confer calcium-activated conductance to *Xenopus* oocytes but has not been characterized (25). We expressed the olfactory form of mouse ANO2 in HEK-293 cells and conducted patch-clamp analysis. The cells were co-transfected with a plasmid expressing the olfactory CNG channel subunit CNGA2, enabling us to activate selectively either a cationic cAMP-gated conductance or a putative Ca^{2+}-activated anion conductance in the patch. The cAMP-gated conductance aided in identifying the inside-out patch configuration and served as a control of patch integrity over time (see Fig. 3*A*). Experiments were performed in 140-mM symmetrical NaCl solutions. The patches were stimulated with Ca^{2+} or cAMP at concentrations that yield a maximal open probability for the native olfactory CaCC and a CNGA2 homomeric channel, respectively (9, 26).

To test whether ANO2 confers a Ca^{2+}-activated conductance to HEK-293 membranes, the patch was exposed to 1 mM Ca^{2+} immediately following excision. Indeed, Ca^{2+} elicited a rapidly peaking current (Fig. 3*A*). The current showed marked inactivation during the 3-s Ca^{2+} exposure and terminated rapidly after Ca^{2+} was removed. Repeated stimulation revealed a continuing rundown of peak current over time (Fig. 3*A* and Fig. S5). This current rundown was not caused by compromised patch integrity (e.g., patch size and access), because the cAMP-elicited current, which also was recorded following each Ca^{2+} stimulation, remained stable during the entire recording duration (Fig. 3*A* and Fig. S5). Rundown of the Ca^{2+}-activated Cl^- current over time is a well-documented property of the native olfactory CaCC (9). We analyzed the rundown of the ANO2 Ca^{2+}-activated current in 11 patches that had sufficiently large Ca^{2+}-activated currents and were stable for at least 12 min as judged by the cAMP-activated current. The ANO2 Ca^{2+}-activated current exhibited 56% rundown over the time course of the experiment (Fig. S5), similar to the 52% rundown observed in the native olfactory CaCC (9). In the control experiments, in which HEK-293 cells were transfected with plasmids encoding CNGA2 and EGFP, only small and noisy calcium-activated currents were observed occasionally. These currents were activated with a considerable delay of a few seconds and disappeared within 1–2 min.

To investigate if the channel formed by ANO2 is indeed a Cl^- channel, we recorded current–voltage (I–V) relationships. In symmetrical NaCl solutions, the ANO2 channel current reversed at a potential close to 0 mV (Fig. 3*B*), with slight inward rectification similar to the native olfactory CaCC (9). When 130 mM (of 140 mM) NaCl in the bath was replaced by Na-methanesulfonate, the reversal potential shifted to -34.6 ± 1.7 mV ($n = 6$), demonstrating that this current is indeed carried by Cl^-. The relative permeability P_{MeS}/P_{Cl} was determined to be 0.17 ± 0.02.

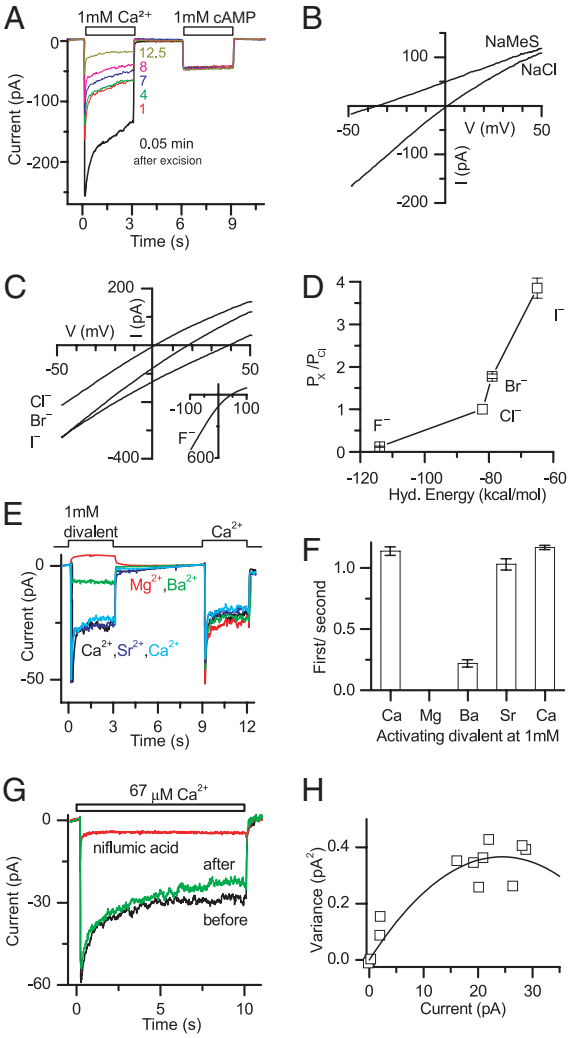

Fig. 3. Biophysical properties of ANO2 channel. (*A*) Heterologously expressed ANO2 confers a Ca^{2+}-activated conductance that runs down over time. Recording of an inside-out patch exposed to 1 mM Ca^{2+} followed by 1 mM cAMP. Repeated Ca^{2+} and cAMP application demonstrates the progressive reduction (''rundown'') of the Ca^{2+}-activated current while the CNG current remains constant. The times beside each trace denote the minutes after patch excision. Holding potential was −40 mV. For quantification of the rundown, see Fig. S5. (*B*) I−V relationships of ANO2. The channel was activated with 67 μM and 100 μM Ca^{2+}, respectively. NaCl trace, symmetrical NaCl solutions; NaMeS trace, methanesulfonate-negative replacement of Cl^- in bath. (*C* and *D*) Halide permeability of the ANO2 channel. (*C*) I−V relationships from a patch where the bath solution contained 140 mM NaCl, NaBr, or NaI. The pipette contained 140 mM NaCl. (*Inset*) I–V relationships from a patch where the pipette solution contained 130 mM NaF and 10 mM NaCl. The bath contained 140 mM NaCl and 67 μM Ca^{2+}. (*D*) Halide permeability as a function of hydration energy. (*E* and *F*) Activation of ANO2 by divalent cations. (*E*) Current traces of ANO2-containing patches activated by 1 mM Ca^{2+}, Mg^{2+}, Ba^{2+} and Sr^{2+}. The small shift in current observed during Mg^{2+} application is not understood but might be caused by a change in seal resistance. (*F*) The ratio of the first peak response to the second. The current elicited by each test divalent was normalized to the Ca^{2+}-elicited current recorded in close time proximity to minimize the effect of the rundown. (*G*) Niflumic acid (300 μM) greatly reduces ANO2 Ca^{2+}-activated current. This inhibition is reversible. (*H*) Noise analysis of the data in Fig. 4*A*. The variance (see *Material and Methods*) was plotted against the current and fitted with $\sigma^2 = iI - I^2/N$, with i = 0.03 pA and $n = 1640$.

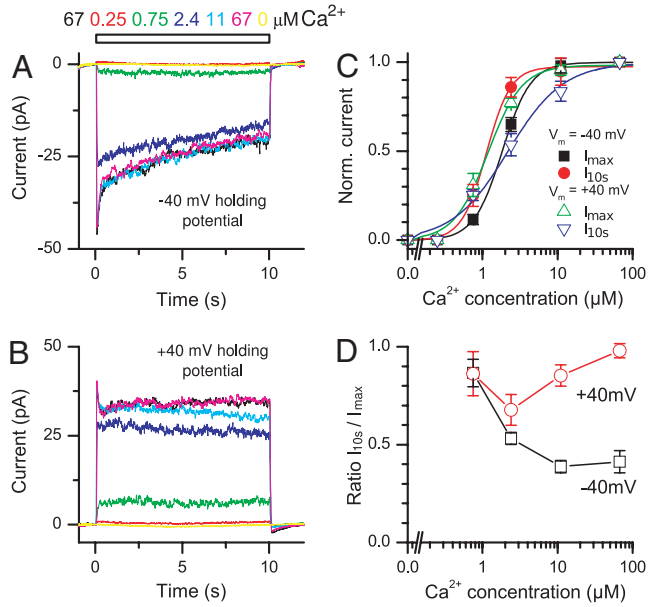

Fig. 4. Ca^{2+} Dose dependency and inactivation kinetics of the ANO2 channel. (*A* and *B*) A patch was exposed for 10 s to a series of Ca^{2+} concentrations at −40 mV (*A*) and +40 mV (*B*). (*C*) The peak current and the current at 10 s were plotted against the Ca^{2+} concentration for both −40-mV and +40-mV holding voltages and fitted with Hill functions. (*D*) The ratio of the current at 10 s to the peak current showed a marked decline at −40 mV with increasing Ca^{2+} concentration but not at +40 mV.

The native olfactory CaCC has been documented to exhibit varying permeabilities to different halide ions (9). We therefore investigated the halide permeability of the ANO2 channel by equimolar replacement of bath NaCl by NaBr or NaI. This replacement progressively shifted the I–V relationships to the right and the reversal potentials to more positive values (Fig. 3*C*), indicating that the ANO2 channel is more permeable to both Br^- and I^- than it is to Cl^-. In the case of F^-, to avoid Ca^{2+} chelation by fluoride in the bath, 130 mM NaCl was replaced equimolarly with NaF in the pipette solution. The reversal potential was shifted to more positive values (Fig. 3*C Inset*), now indicating that the ANO2 channel is less permeable to F^- than to Cl^-. The reversal potentials and the Goldman-Hodgkin-Katz equation yielded a permeability sequence of $I^- > Br^- > Cl^- > F^-$ and permeability ratios P_X/P_{Cl} of 3.85:1.78:1:0.12 ($n = 6$ for Br^- and I^-, $n = 7$ for F^-), which are inversely related to the hydration energies (Fig. 3*D*). These relative halide permeabilities are very similar to the native olfactory CaCC (9) (Table S2).

The native olfactory CaCC has been documented to exhibit varying sensitivities to different divalent cations (9). We tested the activation of the ANO2 channel by other divalents. Because ANO2 currents showed rundown, we first exposed the patch to the test divalent at 1 mM followed by an exposure to 1 mM Ca^{2+} (Fig. 4*E*). This procedure enabled us to normalize the response of the test divalent to the Ca^{2+}-evoked current in each trial. Sr^{2+} activated the ANO2 channel almost as well as Ca^{2+}, Ba^{2+} was only a poor agonist, and no current was observed upon Mg^{2+} application (Fig. 4*G*, $n = 5$). These observations for the ANO2 channel are consistent with those for the native olfactory CaCC (9) (Table S2).

We also tested the sensitivity of the ANO2 channel to niflumic acid, a routinely used blocker of the native olfactory CaCC (8, 9). Niflumic acid (300 μM) substantially reduced patch currents by 77% ± 5% ($n = 8$) when applied simultaneously with Ca^{2+} (Fig. 3*G*).

We attempted to obtain the single-channel conductance for the ANO2 channel. Because the low conductance of individual ANO2 channels hinders direct measurement, we used noise analysis (Fig. 3*H*). The single-channel conductance was esti-

NEUROSCIENCE

mated to be 0.8 ± 0.1 picosiemens (pS) ($n = 5$) by the parabolic fit and 1.22 ± 0.08 pS by the more accurate linear fit (see *Materials and Methods*). These values are similar to that of the native olfactory CaCC, 1.27 pS (9) (Table S2).

We further investigated the sensitivity of ANO2 to Ca^{2+} by exposing patches for 10 s to increasing Ca^{2+} concentrations at both −40-mV and +40-mV holding potentials (Fig. 4 *A* and *B*). The experiments were performed ≈10 min after patch excision to allow completion of the more rapid phase of the current rundown. We determined the dose-dependency (Fig. 4*C*) for the peak current (I_{max}) and for the current at 10 s (I_{10s}), similar to the analysis performed for the native olfactory CaCC (9). The current at 10 s was used to evaluate a change in Ca^{2+} sensitivity during the inactivation. The data were fit with Hill functions. When comparing I_{max}, the $K_{1/2}$ were 1.83 μM ($n = 5$) at −40 mV (Fig. 4*C*, *black curve*) and 1.18 μM ($n = 4$) at +40 mV (Fig. 4*C*, *green curve*), indicating a higher apparent Ca^{2+} affinity at positive holding potentials. This finding is consistent with observations in the native olfactory CaCC (9). Hill coefficients were 2.3 at −40 mV and 1.92 at +40 mV. However, when comparing the current after inactivation (I_{10s}), the dose dependency showed the opposite trend. The $K_{1/2}$ were 1.12 μM at −40 mV (Fig. 4*C*, *red curve*) and 2.18 μM at +40mV (Fig. 4*C*, *blue curve*), indicating that after inactivation ANO2 actually was more sensitive to Ca^{2+} at −40 mV that at +40 mV. The dose–response also was much shallower at +40 mV (Hill coefficients were 2.67 at −40 mV and 1.18 at +40 mV). Overall, the Ca^{2+} sensitivities of the ANO2 channel are comparable to those of the native olfactory CaCC (4, 9) (Table S2).

The kinetics of ANO2 channel inactivation were found to be quite different at positive and negative holding potentials. At −40 mV and at high Ca^{2+} concentrations, ANO2 currents typically showed a rapid inactivation during the first 1 s of Ca^{2+} application followed by a steady decline thereafter (Fig. 4*A*). These inactivation kinetics are comparable to the native olfactory CaCC (9). However, the steady secondary decline of the ANO2 current was minimal at +40 mV (Fig. 4*B*), unlike the native olfactory CaCC, which also displays a steady secondary inactivation at +40 mV (9). We quantified the level of inactivation during Ca^{2+} stimulation by dividing I_{10s} by its respective I_{max} (Fig. 4*D*) for each Ca^{2+} concentration. At low Ca^{2+} levels, currents showed little inactivation regardless of holding potential. Inactivation became more apparent and severe at higher Ca^{2+} concentrations at −40 mV, whereas at +40 mV the I_{10s}/I_{max} ratio decreased only slightly with increasing Ca^{2+} concentrations and recovered to almost 1 at saturating Ca^{2+} concentrations. For the ANO2 channel, the difference in inactivation kinetics between positive and negative holding potentials partly explains the reduction in the Hill coefficient for the I_{10s} dose–response at +40 mV in Fig. 4*C*. Note that the rapid inactivation of the current at the onset of Ca^{2+} exposure was observed in some, but not all, patches obtained from native OSNs (9), probably because patches from OSNs often contain long, thin cilia that slow solution exchange and thus slow the activation of the current.

Taken together, the patch-clamp experiments on heterologously expressed ANO2 channels show that ANO2 forms a calcium-activated chloride channel with properties remarkably similar to the native olfactory CaCC in terms of rundown, slight permeability to Na-methanesulfonate, halide permeability sequence, divalent cation activation, inhibition by niflumic acid, single-channel conductance, biphasic inactivation at negative holding potentials, and Ca^{2+} sensitivity (4, 8, 9). Table S2 shows a comparison of ANO2 and native olfactory CaCC properties.

Discussion

In this study, we identified ANO2 from a proteomic screen of an olfactory cilial membrane preparation. The nature of mass spectrometry-based proteomics is biased toward the identification of abundant proteins. Therefore, the identification of all known olfactory transduction components downstream of ORs in our proteomic screen exemplifies that OSN cilia are a highly specialized compartment for sensory signaling. Although we intentionally separated a gel band for 35- to 55-kDa proteins with the consideration of the presence of a large number of ORs, mass spectrometry did not identify any ORs in any fraction (Table S1), presumably because of the high diversity and very low abundance of individual ORs in the preparation. We tailored our proteomic analysis toward the identification of CaCC candidate(s), based on the hypotheses that the olfactory CaCC is enriched in the cilial membrane and that the CaCC might have a relatively high molecular weight. Using these criteria, we were able to focus on a small list of proteins to select ANO2 as a CaCC candidate. Previously, 2 proteomic analyses of rat olfactory cilial preparations were reported. In the first report, ANO2 and even adenylyl cyclase III (ACIII) were not found (27). In the second report, ANO2 was found among 377 proteins (28).

The close similarity of ANO2 channel properties to the native olfactory CaCC strongly suggests that ANO2 is a major, if not sole, component of the olfactory CaCC. However, because we found a few minor differences, we cannot rule out the possibility that an additional regulatory subunit is present in the native channel, as has been suggested for ANO1 (25). Nevertheless, ANO2 most likely is the pore-forming subunit. Although RT-PCR analysis of nasal tissue, which contains various cell types, for all *Ano* family members shows amplification of a few *Ano* genes (Fig. S6 and Table S3), ANO2 was the only ANO protein found in our proteomic screen. Additionally, no other *Ano* family member transcripts have been found to be OSN-specific (20). Bestrophin 2 (Best2) has been proposed as a candidate olfactory CaCC (29). However, we did not detect any peptides matching Best2 protein in our screen of olfactory cilial membranes. Also, some channel properties of Best2 differ from the native olfactory CaCC. Further, *Best2*$^{-/-}$ mice have been shown to perform an olfactory behavior test normally (30).

The gating mechanism of the native olfactory CaCC is unknown. Although calcium alone is sufficient to open the native olfactory CaCC in patch-clamp experiments (9), the loss of Cl^- channel activity over time after patch excision (“rundown”) is consistent with the loss of a modulatory factor. A study performed using the OSN-like cell line *Odora* implicated calmodulin in the gating mechanism of the native olfactory CaCC (31). Further, other regulatory mechanisms affecting the olfactory CaCC, such as phosphorylation and membrane trafficking, have not yet been explored. With the identification of ANO2 as the major component of the olfactory CaCC, these questions can be addressed directly by site-directed mutagenesis and protein-interaction studies.

Different members of channel families often have different biophysical properties, making them more suited for their roles in their specific cell type. Comparison of heterologously expressed ANO1 and ANO2 channels shows substantial differences in their channel properties, even though they share a similar order of relative halide permeabilities (23, 25). ANO1 channels seem to have a higher sensitivity to Ca^{2+}, certainly at positive holding potentials (23, 24). ANO1 channels also have much slower opening and closing kinetics (23) when exposed to Ca^{2+}. A channel with such slow kinetics acts like a low-pass filter, a characteristic possibly better suited for secretion but not for rapidly signaling in neurons. Finally, the single-channel conductance for ANO1 was reported to be 8.3 pS (23), a value around 8 times larger than we found for ANO2 and for the native olfactory CaCC (9). A small chloride-channel conductance is important in olfactory transduction to convey the low-noise amplification of the primary CNG current (11). Thus, the ANO2 channel is well suited for its role in olfactory signal transduction.

It is tempting to speculate that animals lacking ANO2 may have significantly reduced sensitivity to odors. In humans, the full-length ANO2 is not present in patients who have von Willebrand's disease type 3, where a 253-kb deletion in chromosome 22 results in the deletion of the gene encoding von Willebrand's factor—a protein involved in blood clot formation—and the deletion of the N terminus of the neighboring *Ano2* gene (32). In an interview with the widow of a patient homozygous for this mutation, it was found that "1) her husband never complained about the meals even if they were burnt. 2) When [the patient] was cooking he was possibly not noticing when the potatoes were burnt. 3) [His] use of perfume was sometimes so extreme that his wife wondered how he could stand it. 4) He never mentioned the smell of flowers or 'rural' smells." (Drs. Roswitha Eisert and Reinhard Schneppenheim, personal communication).

In addition to mediating amplification in the olfactory system, ANO2 might play roles in other neuronal systems. For instance, ANO2 transcripts have been found in the retina (NCBI), and in brain regions such as the inferior olivary complex of the brainstem and the cerebral lateral septal nucleus (Allen Brain Atlas). Other ANO family members have even broader expression in several tissues and across development (23–25, 33, 34) and have been proposed as mediators of physiological functions ranging from epithelial secretion to smooth muscle contraction (16). The role of ANO2 in the olfactory system will elucidate the diverse functions of calcium-activated chloride conductance brought about by this recently characterized protein family.

Materials and Methods

Mice were handled and euthanized with methods approved by the Animal Care and Use Committees of The Johns Hopkins University.

Olfactory Cilial Membrane Preparation and Protein Analysis by LC-MS/MS. Olfactory cilia from 30 mice were isolated by the calcium shock method (35). The cilia were treated with hypotonic solution (36) followed by ultracentrifugation over a sucrose gradient to isolate membranes. The membrane-enriched sucrose fractions were pooled, and the proteins were separated by SDS/PAGE. The gel was cut into 3 sections and stored in water. The slices were processed and analyzed by LC-MS/MS by the Taplin Mass Spectrometry Facility (Harvard University). For details, see *SI Methods*.

Molecular Characterization of *Ano2*. For details on RT-PCR, in situ hybridizations, fusion protein expression, and viral construction, see *SI Methods*.

Patch-Clamp Analysis. Mouse olfactory ANO2 was co-expressed with CNGA2 in HEK-293 cells. Recordings from inside-out patches (see *SI Methods* for details) were performed essentially as described (9). For estimation of single-channel conductance by noise analysis, the data were fit with the parabolic function $\sigma^2 = iI - I^2/N$, where i is the single-channel conductance, N is the total number of channels in the patch, and I is the mean current (37), assuming the channel has no subconductances. Because the current showed rapid inactivation after its peak, the variance for high current values could not be determined reliably: digital high-pass filtering introduced wave-like artifacts during fast current changes (''ringing''). Also, the calculation of the mean current during the 0.5-s variance measurement interval would be questionable during rapidly changing currents. Typically, only after the current settled to around half its maximal value could the variance be determined. This limitation affected our ability to fit the entire parabola, but nevertheless the single-channel conductance was determined. A more accurate calculation was performed by fitting only small current values (typically the first 2 data points) with the linear function $\sigma^2 = iI$.

ACKNOWLEDGMENTS. We thank Drs. Roswitha Eisert and Reinhard Schneppenheim for their interview of the widow of the late patient who had the VWF mutation regarding his olfactory abilities. We thank K. Cunningham, D. Fambrough, S. Hattar, E. Kozub, and R. Kuruvilla for suggestions and discussions and H. Ozdener for help with cell culture. We thank the members of the Hattar-Kuruvilla-Zhao mouse tri-lab of the Johns Hopkins Department of Biology for discussions. This work was supported by National Institutes of Health Grant DC007395, the Monell Chemical Senses Center, and a Morley Kare Fellowship (to J.R.).

1. Firestein S (2001) How the olfactory system makes sense of scents. *Nature* 413:211–218.
2. Kleene SJ (2008) The electrochemical basis of odor transduction in vertebrate olfactory cilia. *Chem Senses* 33:839–859.
3. Kaneko H, Putzier I, Frings S, Kaupp UB, Gensch T (2004) Chloride accumulation in mammalian olfactory sensory neurons. *J Neurosci* 24:7931–7938.
4. Reisert J, Lai J, Yau KW, Bradley J (2005) Mechanism of the excitatory Cl− response in mouse olfactory receptor neurons. *Neuron* 45:553–561.
5. Nickell WT, Kleene NK, Kleene SJ (2007) Mechanisms of neuronal chloride accumulation in intact mouse olfactory epithelium. *J Physiol (Paris)* 583:1005–1020.
6. Kleene SJ, Gesteland RC (1991) Calcium-activated chloride conductance in frog olfactory cilia. *J Neurosci* 11:3624–3629.
7. Kurahashi T, Yau K-W (1993) Co-existence of cationic and chloride components in odorant-induced current of vertebrate olfactory receptor cells. *Nature* 363:71–74.
8. Kleene SJ (1993) Origin of the chloride current in olfactory transduction. *Neuron* 11:123–132.
9. Reisert J, Bauer PJ, Yau KW, Frings S (2003) The Ca-activated Cl channel and its control in rat olfactory receptor neurons. *J Gen Physiol* 122:349–363.
10. Lowe G, Gold GH (1993) Nonlinear amplification by calcium-dependent chloride channels in olfactory receptor cells. *Nature* 366:283–286.
11. Kleene SJ (1997) High-gain, low-noise amplification in olfactory transduction. *Biophys J* 73:1110–1117.
12. Boccaccio A, Menini A (2007) Temporal development of cyclic nucleotide-gated and Ca2+ -activated Cl− currents in isolated mouse olfactory sensory neurons. *J Neurophysiol* 98:153–160.
13. Su T, Ding X (2004) Regulation of the cytochrome *P450 2A* genes. *Toxicol Appl Pharmacol* 199:285–294.
14. Nishizawa T, Nagao T, Iwatsubo T, Forte JG, Urushidani T (2000) Molecular cloning and characterization of a novel chloride intracellular channel-related protein, parchorin, expressed in water-secreting cells. *J Biol Chem* 275:11164–11173.
15. Gherman A, Davis EE, Katsanis N (2006) The ciliary proteome database: An integrated community resource for the genetic and functional dissection of cilia. *Nat Genet* 38:961–962.
16. Hartzell HC, Yu K, Xiao Q, Chien LT, Qu Z (2008) Anoctamin/TMEM16 family members are Ca2+-activated Cl− channels. *J Physiol* 587:2127–2139.
17. Tsutsumi S, et al. (2004) The novel gene encoding a putative transmembrane protein is mutated in gnathodiaphyseal dysplasia (GDD). *Am J Hum Genet* 74:1255–1261.
18. Kornak U, et al. (2001) Loss of the ClC-7 chloride channel leads to osteopetrosis in mice and man. *Cell* 104:205–215.
19. Entian KD, et al. (1999) Functional analysis of 150 deletion mutants in *Saccharomyces cerevisiae* by a systematic approach. *Mol Gen Genet* 262:683–702.
20. Yu T-T, et al. (2005) Differentially expressed transcripts from phenotypically identified olfactory sensory neurons. *J Comp Neurol* 483:251–262.
21. Juschke C, Wachter A, Schwappach B, Seedorf M (2005) SEC18/NSF-independent, protein-sorting pathway from the yeast cortical ER to the plasma membrane. *J Cell Biol* 169:613–622.
22. Strotmann J, Levai O, Fleischer J, Schwarzenbacher K, Breer H (2004) Olfactory receptor proteins in axonal processes of chemosensory neurons. *J Neurosci* 24:7754–7761.
23. Yang YD, et al. (2008) TMEM16A confers receptor-activated calcium-dependent chloride conductance. *Nature* 455:1210–1215.
24. Caputo A, et al. (2008) TMEM16A, a membrane protein associated with calcium-dependent chloride channel activity. *Science* 322:590–594.
25. Schroeder BC, Cheng T, Jan YN, Jan LY (2008) Expression cloning of TMEM16A as a calcium-activated chloride channel subunit. *Cell* 134:1019–1029.
26. Bradley J, Reuter D, Frings S (2001) Facilitation of calmodulin-mediated odor adaptation by cAMP-gated channel subunits. *Science* 294:2176–2178.
27. Mayer U, et al. (2008) proteomic analysis of a membrane preparation from rat olfactory sensory cilia. *Chem Senses* 33:145–162.
28. Mayer U, et al. (2009) The proteome of rat olfactory sensory cilia. *Proteomics* 9:322–334.
29. Pifferi S, et al. (2006) Bestrophin-2 is a candidate calcium-activated chloride channel involved in olfactory transduction. *Proc Natl Acad Sci USA* 103:12929–12934.
30. Bakall B, et al. (2008) Bestrophin-2 is involved in the generation of intraocular pressure. *Invest Ophthalmol Visual Sci* 49:1563–1570.
31. Kaneko H, Mohrlen F, Frings S (2006) Calmodulin contributes to gating control in olfactory calcium-activated chloride channels. *J Gen Physiol* 127:737–748.
32. Schneppenheim R, et al. (2007) A common 253-kb deletion involving VWF and TMEM16B in German and Italian patients with severe von Willebrand disease type 3. *Journal of Thrombosis and Haemostasis* 5:722–728.
33. Rock JR, Harfe BD (2008) Expression of *TMEM16* paralogs during murine embryogenesis. *Dev Dyn* 237:2566–2574.
34. Gritli-Linde A, et al. (2009) Expression patterns of the *Tmem16* gene family during cephalic development in the mouse. *Gene Expression Patterns* 9:178–191.
35. Anholt RR, Aebi U, Snyder SH (1986) A partially purified preparation of isolated chemosensory cilia from the olfactory epithelium of the bullfrog, *Rana catesbeiana*. *J Neurosci* 6:1962–1969.
36. Adoutte A, et al. (1980) Biochemical studies of the excitable membrane of *Paramecium tetraurelia*. III. Proteins of cilia and ciliary membranes. *J Cell Biol* 84:717–738.
37. DeFelice LJ (1981) *Introduction to Membrane Noise* (Plenum Press, New York).